Thermodynamic Profiling of Peptide Membrane Interactions by Isothermal Titration Calorimetry: A Search for Pores and Micelles

J. R. Henriksen and T. L. Andresen*
Department of Micro- and Nanotechnology, Technical University of Denmark, Lyngby, Denmark

ABSTRACT Antimicrobial peptides are known to interact strongly with negatively charged lipid membranes, initially by peripheral insertion of the peptide into the bilayer, which for some antimicrobial peptides will be followed by pore formation, and successive solubilization of the membranes resulting in mixed peptide-lipid micelles. We have investigated the mode of action of the antimicrobial peptide mastoparan-X using isothermal titration calorimetry (ITC) and cryo-transmission electron microscopy (cryo-TEM). The results show that mastoparan-X induces a range of structural transitions of POPC/POPG (3:1) lipid membranes at different peptide/lipid ratios. It has been established that ITC can be used as a fast method for localizing membrane transitions and when combined with DLS and cryo-TEM can elucidate structural changes, including the threshold for pore formation and micellation. Cryo-TEM was employed to confirm the structural changes associated with the thermodynamic transitions found by ITC. The pore-formation process has furthermore been investigated in detail and the thermodynamic parameters of pore formation have been characterized using a system-specific temperature where the enthalpy of peptide partitioning becomes zero (T_{zero}). This allows for an exclusive study of the pore-formation process. The use of ITC to find T_{zero} allows for characterization of the thermodynamic parameters of secondary processes on lipid membranes.

INTRODUCTION

Antimicrobial peptides (AMPs) have received increasing attention as an increasing number of multiresistant bacteria makes the search for new potential antibiotics imperative. AMPs are naturally occurring peptides and have been isolated from frog skin (magainins), wasp venom (mastoparans), bee venom (melittin), and silk moths (cecropins). These peptides can be divided into several groups, including 1), the linear and α-helical, 2), the cyclic, and 3), the β-sheet forming peptides. All share common features in that they are cationic, possess large hydrophobic moments, and upon interaction with lipid membranes undergo conformational changes. Examples are the canonical linear peptides, melittin and magainin-II, which changes conformation from unstructured to α-helical in the presence of lipid membranes (1,2). As all of these peptides are made up of hydrophilic and hydrophobic residues they easily distribute between aqueous and lipid phases. The fact that this distribution/partitioning is biased toward negatively charged lipid membranes due to favorable electrostatic interactions is believed to be a cornerstone in AMP selectivity between mammalian or bacterial cell membranes (3). A second factor that regulates the selectivity of AMPs is the high content of cholesterol in mammalian cell membranes, which causes a tighter packing of lipids in the bilayer, thereby abolishing/hampering the insertion of peptides (4,5).

Upon membrane partitioning, AMPs embed into the region of the lipid headgroup (Fig. 1), which decreases the lipid packing and causes thinning of the bilayer (6,7). This ultimately leads to a lowering of the diffusion barrier constituted by the membrane and consequently to an increased exchange of ions across the bilayer. In a number of studies, a second mode of action has been reported, wherein the peptide changes behavior, leading to the formation of pores (2,8–11) (Fig. 1) or disruption of the bilayer and formation of mixed peptide-lipid micelles (12). The onset of pore formation has furthermore been shown to occur in a cooperative manner when a critical peptide/lipid ratio, $(P/L)^*$, has been reached (13). Formation of pores or micelles leads to perforation of the cell membrane, which causes exchange of ions and nutrition molecules across the lipid bilayer, leading to cell death (14). Alternative modes of action exhibited by some AMPs are membrane translocation (15,16) and lipid clustering (17,18). These modes of action, in which the peptide targets the lipid membrane, are believed to be responsible for AMP potency toward various cell types, in particular bacteria.

Several studies have been undertaken to shed light on the nature of the processes occurring above the (P/L)*, and the results have shown that the AMPs can be divided into two categories: pore-forming and membrane-solubilizing (3). In particular, the structure of peptide pores has been studied intensively using small-angle neutron scattering, small-angle x-ray scattering, fluorescence, and, recently, cryo-transmission electron microscopy (cryo-TEM), and the presence of pores has been reported for a number of AMPs, including mastoparan-X (19), melittin (9,10), magainin (20,21) and alamethicin (22). Although much is known about the structure of these peptide-lipid assemblies, less is known about the critical threshold at which they occur. So far, $(P/L)^*$ values have been published for only a limited number of peptides, e.g., magainin, melittin, and alamethicin, and lipid membranes, making it difficult to compare their modes of

Submitted September 10, 2010, and accepted for publication May 4, 2011.

*Correspondence: thomas.andresen@nanotech.dtu.dk

Editor: Heiko H. Heerklotz.

0006-3495/11/07/0100/10 $2.00

doi: 10.1016/j.bpj.2011.05.047

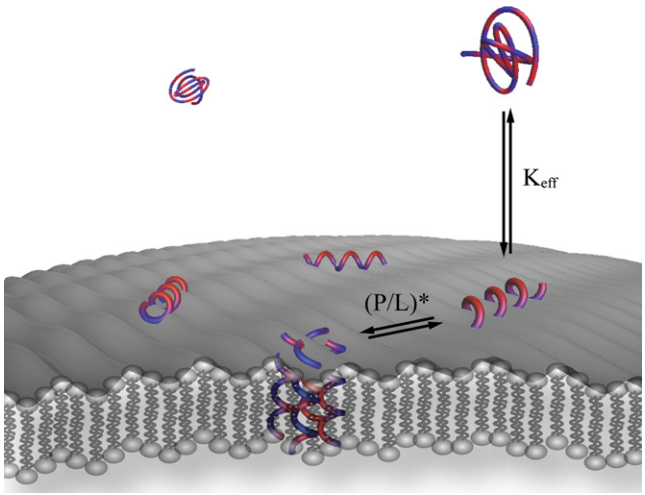

FIGURE 1 Illustration of an amphipathic peptide interacting with a lipid membrane. The peptide, which is shown in alternating blue and red to illustrate hydrophobic and hydrophilic amino acid residues, respectively, initially partitions onto the lipid membrane resulting in a conformational change of the peptide. Above the critical peptide/lipid ratio, $(P/L)^*$, the peptide inserts into the membrane and forms a pore. The insertion and pore formation are governed by the effective partition coefficient (K_{eff}) and the pore-formation threshold $(P/L)^*$.

action and biological effects on cells. The current reports of $(P/L)^*$ are mainly based on x-ray diffraction, oriented circular dichroism (6,23,24), and fluorescence (9,10,19,25). These techniques require either specialized instrumentation (x-ray or neutron facilities) or specific sample preparation, e.g., encapsulation of fluorescence probes that may affect the membrane, thus limiting the number of systems that can be investigated. A simple and noninvasive method for screening the mode of action of the peptides and resolving the critical threshold, $(P/L)^*$, at which the structural transitions occur, is thus highly desirable.

Research in partitioning of peptides onto lipid membranes has been intense for several years. Along with scattering techniques and NMR, isothermal titration calorimetry (ITC) has proven to be a powerful tool for thermodynamic characterization of peptide-membrane interactions. In this study, inspired by the work of Wenk and Seelig (8) and Heerklotz and co-workers (26), we introduce a new, to our knowledge, method for determining the onset of pore formation and membrane micellation. This method is based on ITC, and the detection principle thus relies on the heat of reaction, which is an intrinsic property of the interaction of peptides with lipid membranes. Mastoparan-X (MPX), a 14-residue antimicrobial peptide isolated from the venom of *Vespa xanthoptera* (27) has been used as a model AMP in the development of the ITC-based methodology. MPX carries four positive charges and interacts strongly with POPC and POPC/POPG (3:1) lipid membranes (28,29). The results presented here show that MPX induces a range of structural transitions of POPC/POPG (3:1) membranes at different peptide/lipid ratios. It has been established that ITC can be used to elucidate the threshold where transitions occur, including the threshold for pore formation and micellation. The structural changes have been investigated by dynamic light scattering (DLS), static light scattering (SLS), and cryo-TEM. We have further investigated the pore formation in detail and found that the thermodynamic parameters of pore formation can be characterized using a system-specific temperature at which the enthalpy of peptide partitioning becomes zero (T_{zero}). This allows for an exclusive study of the pore-formation process.

MATERIALS AND METHODS

Materials

POPC (1-palmitoyl-2-oleoyl-*sn*-glycero-3-phosphocholine) and POPG (1-palmitoyl-2-oleoyl-*sn*-glycero-3-phospho-(1′-*rac*-glycerol) (sodium salt)) were obtained from Avanti Polar Lipids (Alabaster, AL). Mastoparan-X (H-Ile-Asn-Trp-Lys-Gly-Ile-Ala-Ala-Met-Ala-Lys-Lys-Leu-Leu-NH2) was synthesized as described previously (28). *N*-(2-hydroxyethyl) piperazine-*N*′-(2-ethanesulfonic acid) (HEPES) and the corresponding sodium salt (HEPES-Na) were purchased from Sigma-Aldrich (Brøndby, Denmark). NaCl was purchased from J. T. Baker Chemicals (Mallinckrodt Baker, Griesheim, Germany). Organic solvents were products of Sigma-Aldrich. All materials were used without further purification.

Sample preparation

LUV preparation

Lipid stock solutions of POPC and POPG were prepared in chloroform/methanol (9:1). Mixtures of POPC/POPG (3:1) were prepared, and the organic solvent was evaporated under a gentle stream of argon. The lipid films were kept in vacuum ($P < 0.1$ Pa) overnight to remove the residual solvent. Buffer containing 10 mM HEPES and 100 mM NaCl (pH 7.4) was added to the lipid films, and they were hydrated for 60 min and then extruded through 100 nm using an Avanti mini-extruder. The size distribution of the LUVs was checked by DLS (ZetaPALS, Brookhaven Instruments, Holtsville, NY), and the effective lipid concentration was determined by inductively coupled plasma atomic emission spectroscopy (Vista AX, Varian, Palo Alto, CA).

Peptide stock solutions

Peptide stock solutions were prepared in a buffer containing 10 mM HEPES and 100 mM NaCl (pH 7.4), and the peptide concentration was determined by UV-VIS (Shimadzu UV-1700, PharmaSpec, Birmingham, United Kingdom) using the molar extinction coefficient of tryptophan ($\varepsilon_{\text{tryptophan,280 nm}} = 5600\ \text{cm}^{-1}\ \text{mol}^{-1}$) (30).

ITC measurements

The heat of partitioning for the insertion of peptides onto lipid membranes was determined by ITC (iTC200, GE Healthcare, Wauwatosa, WI). The experiments were conducted by repeating injections of 5 μL aliquots of peptide solution (100 μM) into 0.75 mM or 7.5 mM lipid large unilamellar vesicle (LUV) solution. The heat of dilution was determined by titration of peptide into the buffer and was subtracted from the heat of partitioning. For determining the heat of partitioning, the condition of low peptide/lipid ratio ($P/L < 0.02$) was used to 1), reduce effects of peptide-peptide interactions; and 2), avoid pore formation or secondary events other than partitioning of the peptide. In addition, full partitioning of the peptide was achieved by the condition $C_{Lip} >> 1/K_{eff}$, K_{eff} being the effective partition coefficient (28).

The heat of partitioning was determined at 10°C, 15°C, 20°C, 25°C, and 30°C (see Fig. 2). The first injection is prone to artifacts and has been discarded from the analysis of the heat of partitioning.

Lipid-into-peptide titration

The formation and disintegration of pores or micelles was studied using ITC by titrating LUVs into peptide solution. The lipid-into-peptide (L-P) titration was conducted at 15°C, 20°C, and 25°C by injecting 25 mM POPC/POPG (3:1) LUVs into 100 μM MPX solution. The heat of dilution was estimated as the average of the last 10 injections (Fig. 3 *A*) and was used for correction of the heat of injection (Q) (Fig. 3 *B*) and the accumulated heat (Q_{acc}) (Fig. 3 *C*). The L-P ITC experiments were conducted as 38 × 1 μL injections into the 204 μL-sized ITC cell.

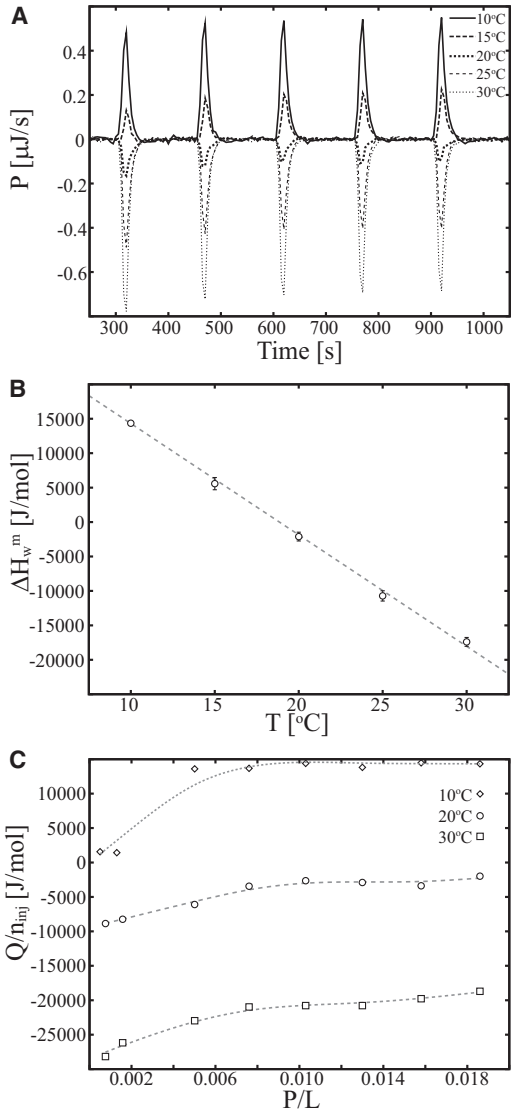

FIGURE 2 Heat of partitioning of MPX onto POPC/POPG (3:1) LUVs resolved by ITC. (*A*) Calorimetric heat traces are shown for the partitioning of MPX as a function of temperature (5 × 5 μL 100 μM MPX injected into 204 μL 0.75 mM LUVs). (*B*) The average molar heat of partitioning, obtained by integration of the calorimetric heat traces shown in *A*. (*C*) The molar heat of partitioning is shown as a function of the peptide/lipid ratio (*P/L*) (n_{inj} is the amount of peptide injected).

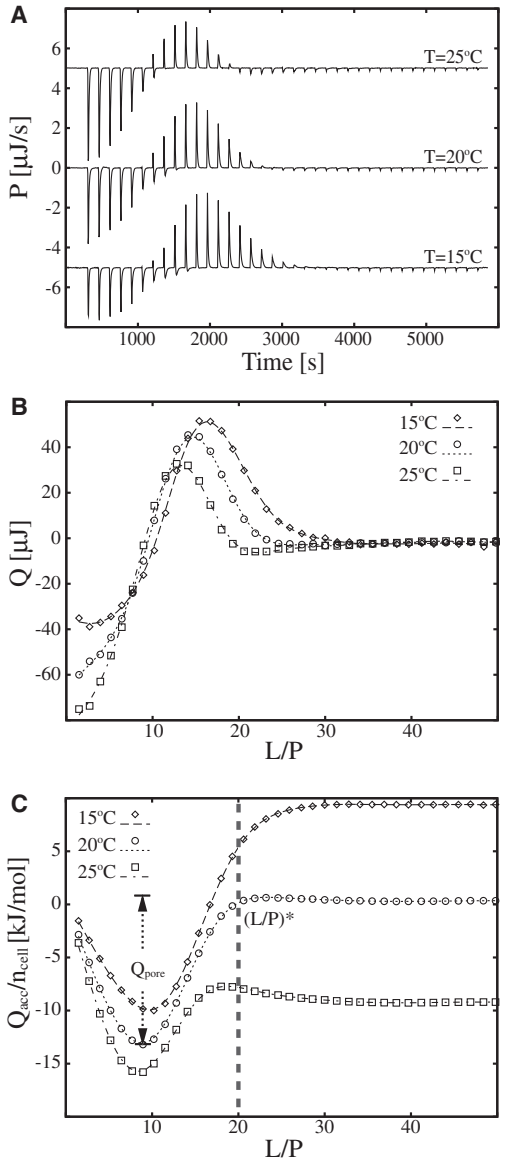

FIGURE 3 ITC heat traces of POPC/POPG (3:1) LUVs injected into MPX solution. (*A*) Calorimetric heat traces of lipid-into-peptide titrations conducted at 15°C, 20°C, and 25°C (38 × 1 μL 18.9 mM POPC/POPG (1:3) injected into 204 μL 100 μM MPX). (*B* and *C*) Integrated heat trace (Q) (*B*) and accumulated molar heat (Q_{acc}/n_{cell}) (*C*) are shown as a function of the lipid/peptide ratio (*L/P*). The threshold (*L/P*)* at which pores cease to exist (or are formed if titrated oppositely) at 20°C, is indicated by a dashed vertical line in *C*. The pore formation energy is denoted by Q_{pore}. The integrated heat of injection (Q_{acc}) in *C* is normalized with respect to the moles of peptide in the ITC cell (n_{cell}). Lines serve to guide the eye.

Peptide-into-lipid titration

The onset of peptide pore formation or membrane micellation was determined using ITC by titration of peptide into LUVs. The titrations were conducted by injecting 250 μM, 500 μM, 1000 μM, or 10 mM MPX solution into 190 μM, 380 μM, 760 μM, or 7.5 mM POPC/POPG (3:1) LUV solution, respectively. The peptide-into-lipid (P-L) ITC experiments were conducted as 38 × 1 μL injections into the 204 μL sized ITC cell.

All ITC experiments were conducted at reference power 5 μCal/s, stirring speed of 1000 rpm, and filter time of 5 s. The acquisition of the ITC

baseline and estimates of peptide and lipid concentrations in the ITC cell were determined using custom-made software as previously described (31).

Cryo-TEM imaging

Electron microscopy studies were performed using a CM120 BioTWIN transmission electron microscope (Philips, Amsterdam, The Netherlands), with a cryo-holder and a cryo-transfer stage. The sample preparation procedure (32) consisted in short of the following. A thin film of sample solution was prepared by a blotting procedure, performed in a custom-built environmental chamber with controlled temperature (25°C) and humidity. A drop of the solution was placed onto a lacy carbon film (black area) supported by a copper grid. Excess solution was removed using filter paper, leaving a thin film of the sample solution to span the holes of the carbon grid. Vitrification of the thin film was achieved by rapidly plunging the grid into liquid ethane (−180°C). The vitrified specimen was subsequently transferred to the microscope. The temperature was kept below −165°C during both the transfer and viewing procedures to prevent sample perturbation and formation of ice crystals. Samples with peptide/lipid ratios of 0, 0.025, 0.06, 0.12, 0.24, and 0.60 were prepared with a final lipid concentration of 7.5 mM. The peptide/lipid ratio 0.24 was prepared and investigated at an additional lipid concentration of 0.75 mM. The samples were equilibrated at ambient temperature for 24 h before vitrification.

Power-spectra calculation

Images of vesicles were manually selected and a region of 256 × 256 pixels was chosen inside the vesicle and outside the vesicle. The images representing the contrast modulation of the vesicle membrane and the aqueous background were Fourier-transformed in 2D using the algorithm fourn (33), and the result was subsequently rotationally averaged. The power spectra are presented as a function of the spatial frequency, S.

RESULTS AND DISCUSSION

ITC offers itself as a noninvasive technique for studying peptide membrane interactions. However, heat signals arising from multiple processes occurring at similar timescales can be difficult to separate, which is the limitation of ITC. Moreover, interpretation of the calorimetric heat traces often requires the use of supplementary techniques to decipher specific calorimetric signatures. This work addresses some of these challenges.

The calorimetric heat trace of peptides injected into lipid membranes, or vice versa, are a complex superposition of heat evolved from several processes occurring in parallel, such as partitioning, pore formation, micellation of the membrane, proton or ion exchange, and heat of dilution. A few of these processes can be resolved individually e.g., the heat of peptide or LUV dilution and the heat of partitioning. In this work, we demonstrate how the temperature dependence of the heat of partitioning can be utilized to reduce the complexity of ITC heat traces where multiple processes are occurring and to elucidate processes such as pore formation and membrane micellation.

Heat of partitioning

The heat of peptide partitioning was investigated using ITC by injection of peptide into a solution containing lipid membrane in great excess. In Fig. 2 *A*, the calorimetric heat trace for the partitioning of MPX onto POPC/POPG (3:1) LUVs is plotted for temperatures in the range 10–30°C, showing 1), a gradual change in the heat trace from endothermic to exothermic as temperature is increased; and 2), trending in the heat trace as a function of the number of injections. The average molar heat of partitioning, $\Delta H_w^m = 1/n \sum Q_i/(V_{inj}C_{inj})$, where n is number of injections included in the average, Q_i is the integrated heat of injection, V_{inj} is the injected volume, and C_{inj} is the concentration of the syringe content, shows the linear dependency, $\Delta H_w^m = 30700 - 1625T[^\circ C]$, when plotted as a function of temperature (Fig. 2 *B*). The molar enthalpies in Fig. 2 *B* are averages of heats acquired in the P/L range 0.01–0.02. At P/L ratios >0.01, the heat of partitioning remains constant, but at low peptide/lipid ratios ($P/L < 0.01$), the heat of partitioning depends on the P/L ratio (Fig. 2 *C*). The P/L dependence of the heat of partitioning indicates nonideal behavior, in accordance with earlier reports for partitioning of detergents into lipid membranes (34). This quantification allows us to determine a zero heat of partitioning at $T_{zeroMPX} = 19^\circ$C (Fig. 2 *B*, valid for $0.01 < P/L < 0.02$). In work by Seelig and co-workers (2), the antimicrobial peptide melittin is shown to have zero enthalpy of partitioning at $T_{zeroMLT} = 28^\circ$C. The temperature at which the enthalpy of partitioning is zero (T_{zero}) depends in general on the investigated system, i.e., the peptide, lipid membrane, and buffer system. In this case, we also observe a dependency on the P/L ratio, which leads to lower estimates of T_{zero} for $P/L < 0.01$. The dependency of T_{zero} on the chosen buffer is caused by contributions from proton exchange between the peptide or membrane and the buffer. Changing to a buffer with a different protonation enthalpy thus provides a method for adjusting T_{zero} to higher or lower temperatures.

Pore formation and disintegration studied by L-P titration

When more than one process is occurring in an ITC experiment, difficulties arise in separating the individual contributions to the calorimetric heat trace, as previously observed by Wenk and Seelig for the case of membrane pore formation (8). In that work, the authors used the excess enthalpy defined with respect to a theoretical partition model to characterize the pore-formation process. In the following, we offer a method that relies only on simple assumptions about the aggregation phenomena. An example is shown in Fig. 3, where the calorimetric heat trace of an L-P titration shows both exothermal and endothermal heat spikes and has a profile that does not resemble the monotonic profile expected for a titration of LUVs into a peptide solution (8). We argue that the calorimetric heat trace shown in Fig. 3 is a superposition of three primary processes: 1), peptide partitioning; 2), a reversible process; and 3), heat

of dilution. The heat evolved can thus be written as $Q = Q_{par} + Q_{rev} + Q_{dil}$, where Q_{par} is the heat of partitioning, Q_{rev} is the heat from the reversible process, which could originate from, e.g., peptide pore formation, membrane micellation, lipid segregation, or peptide clustering, and Q_{dil} is the heat of dilution. In this L-P titration, Q_{dil} is estimated as an average of the heat spikes from the last 10 injections (the process is assumed to be complete in this range). The heat of dilution is subtracted from the calorimetric heat trace.

Conducting ITC experiments at temperatures in the proximity of $T_{zeroMPX} = 19°C$ reduces the complexity of the calorimetric heat trace, since Q_{par} is approximately equal to zero. This effect is observed in Fig. 3 *A* ($T = 20°C$), where the exothermal and endothermal heat traces compensate each other, resulting in an overall accumulated heat close to zero (Fig. 3 *C*). To investigate the nature of the reversible process further, DLS and 90° SLS measurements were conducted for *L/P* ratios 1,10, and 100 (data not presented). These measurements showed no reduction in the hydrodynamic radius of the LUVs or decrease in the SLS signal upon interaction with MPX compared to their respective controls, which indicates that the membrane morphology is unchanged for the process responsible for the ITC trace in Fig. 3. Even though SLS and DLS cannot rule out the existence of a micelle population in the sample, our hypothesis regarding the L-P titration shown in Fig. 3 is that the calorimetric heat trace is governed by the formation and subsequent disappearance of peptide pores; however, peptide aggregates and lipid clusters are also possible. Earlier dye-release studies support the hypothesis of pore formation by MPX (19) and we substantiate it further with our cryo-TEM results later in this report. A similar methodology using ITC in combination with static light scattering was employed by Wenk and Seelig for studies of membrane pore formation by magainin-II amide (8). The sequence of events occurring in Fig. 3 is thus interpreted as initial partitioning of peptide and formation of peptide/lipid pores caused by the large *P/L* ratios leading to exothermic heat spikes. It is noteworthy that the exothermic heat is directly related to the formation of pores, since the heat of partitioning is approximately zero at $T = 20°C$. Throughout the experiment, lipid material is added, leading to increased L/P ratios, and at a certain point ($L/P \sim 9$, $T = 20°C$), the pore-formation process is reversed, leading to a net disruption of pores due to dilution of peptide on the membrane. The disruption of pores is observed as endothermic heat spikes in Fig. 3. At $L/P = 20$ ($T = 20°C$), the pores are fully dissociated, defining the threshold of pore disruption (or threshold of pore formation) on the membrane as $(L/P)^* = 20$. For the L-P titration, it is noteworthy that full partitioning of the peptide is not reached initially and the peptide/lipid ratio on the membrane, $(P/L)_{mem}$, differs from the peptide/lipid ratio of the system, $(P/L)_{sys}$. In general, these ratios are related by $(P/L)_{mem} = K_{eff}C_{lip}/(1 + K_{eff}C_{lip})(P/L)_{sys}$, and consequently, $(P/L)_{mem} << (P/L)_{sys}$ when $K_{eff}C_{lip} << 1$. However, the effective partitioning coefficient, K_{eff}, varies from $6.7 \times 10^3 - 4.1 \times 10^5 M^{-1}$ ($T = 37°C$) (28), depending on the degree of POPG charge neutralization by the cationic MPX peptide, which corresponds to $3.8 \times 10^4 - 2.3 \times 10^6 M^{-1}$ at $T = 20°C$ (estimates based on van't Hoff analysis using partition enthalpies presented in Fig. 2). Depending on the degree of membrane charge neutralization, complete partitioning (>95%) is thus achieved when $C_{lip} > 10–500\ \mu M$ of POPC/POPG (3:1), which is fulfilled at (L/P) ~ 9 in Fig. 3. An immediate consequence of the incomplete partitioning occurring in the initial part of the L-P titration is that $(P/L)_{mem} << (P/L)_{sys}$, which lowers the probability for membrane solubilization in the L-P titration.

At temperatures above or below $T_{zeroMPX}$, the exothermal and endothermal parts of calorimetric heat trace (Fig. 3 *A*) do not compensate each other. This effect is caused by the nonzero heat of partitioning ($Q_{par} \neq 0$), which is evident in Fig. 3 *C*, showing a net positive and net negative accumulated heat at $T < T_{zeroMPX}$ and $T > T_{zeroMPX}$, respectively.

Furthermore, the pore-formation process is exothermal, and estimates for the upper and lower limits of pore-formation enthalpy are $\Delta H^{up} = -19$ kJ/mol and $\Delta H^{low} = -13$ kJ/mol, respectively. The upper limit is calculated as $\Delta H^{up} = Q_{pore}/(C_{pore}V_{cell})$ and lower limit as $\Delta H^{low} = Q_{pore}/(C_{tot}V_{cell})$, where V_{cell} is the ITC cell volume, $Q_{pore} = 260\ \mu J$ is the maximal accumulated pore-formation energy at $T = 20°C$, C_{tot} is the maximum theoretical amount of peptide participating in the pore formation, i.e., 100 μM for the L-P titration, and C_{pore} is an estimate of the minimum amount of peptide participating in pore formation. The latter is estimated by $C_{pore} = K_{eff}C_{lip}/(1 + K_{eff}C_{lip}) \times (C_{tot} - (P/L)^* \times C_{lip}) \sim 70\ \mu M$, where C_{lip} is the lipid concentration at which the pore-formation enthalpy reaches its maximum, which in Fig. 3 corresponds to $C_{lip} \sim 0.65$ mM (upon the seventh injection). The estimate of the lower limit for pore-formation enthalpy is based on the assumption that all of the peptide contributes to the process, and the lower limit on the assumption that only the peptide added beyond the pore onset concentration contributes.

In recent studies by Seelig and co-workers (2), similar ITC heat traces were shown for the interaction of melittin with POPC/POPG (3:1) LUVs, and a pore-formation energy of 9.8 kJ/mol was reported. Noteworthy is the change in the sign of the pore-formation energy, which signifies differences in the lipid-peptide interactions for the formation of pores by melittin and MPX. This effect may be explained by the difference in length between melittin (26 residues) and MPX (14 residues) and thus in their ability to span the lipid bilayer.

Pore formation studied by P-L titration

Pore-formation onset was furthermore studied by reversing the titration in the ITC experiment. MPX peptide was

injected into a solution of LUVs, resulting in variation of the P/L ratio from 0 to 0.25. In the P-L titration, the lipid concentration (C_{Lip}) in the ITC cell is approximately constant (contrary to the reversed P-L titration) and the condition $K_{eff} \times C_{Lip} >> 1$ is fulfilled for the first injection and onward, leading to full partitioning of the peptide. As the amount of peptide per injection is constant, constant heat spikes are anticipated to be the signature of peptide partitioning (assuming zero excess enthalpy of partitioning). Heat spikes of similar size are initially observed, confirming the occurrence of peptide partitioning (Fig. 4 *A*). However, weak trending of the heat spikes are observed as the P/L ratio is increased, which can be hypothesized to be caused by change in the degree of partitioning (caused by augmented membrane charge neutralization as P/L is increased), peptide induced membrane curvature stress, or possible lipid or peptide aggregation on the membrane. As the ratio $P/L = 0.05$ is reached, the calorimetric heat trace changes in a cooperative manner (Fig. 4 *B*, *vertical dashed line*). This ratio is denoted as the pore-formation onset, $(P/L)^* = 0.05$, and it agrees with the pore-disintegration threshold found by L-P titration (Fig. 3 *C*), as is evident by the inverse relationship, $(P/L)^* = 1/(L/P)^*$. In Fig. 4 *B*, the pore-formation onset, $(P/L)^*$, is shown to be independent of the lipid concentration, implying that all peptide is fully bound to the membrane in the concentration range studied, i.e., $(P/L)_{mem} = (P/L)_{sys}$. The reported P/L ratio for the pore-formation onset thus corresponds to the actual composition of the peptide-membrane system. The cooperativity of the pore-formation process depends on C_{Lip}, as revealed by the change in steepness of descent in the calorimetric heat trace beyond $P/L = 0.05$ (see Fig. 4 *B*). When the P/L ratio 0.1 is reached, the magnitude of the calorimetric heat trace decreases, which we hypothesize is due to either 1), a decrease in the net formation of pores due to saturation of the lipid bilayer with respect to insertion of additional peptides caused by peptide-peptide or pore-pore repulsion; or 2), a decrease in the pore-formation enthalpy caused by nonideal behavior.

The P-L titration was furthermore investigated at 20°C, 25°C, and 30°C, as shown in Fig. 4 *C*, revealing an exothermal heat of partitioning in the range $P/L = 0$–0.1, in accordance with the heat-of-partitioning data shown in Fig. 2. The pore-formation threshold is increased as a function of temperature, in agreement with the pore-formation process being exothermal, and the cooperativity of the process is diminished.

The pore-formation onset of melittin has previously been investigated by x-ray diffraction (7), revealing membrane thinning before the formation of pores. In this work, the pore-formation onset of melittin was reported to be $P/L = 0.014$ and 0.025 for di20:1PC and di22:1PC lipid membranes, respectively (7). Melittin thus has a higher propensity for forming pores compared to MPX. Moreover, the pore-formation threshold of melittin was shown to depend on membrane thickness, resulting in lower $(P/L)^*$ ratios for thinner membranes such as POPC/POPG (3:1) lipid membranes.

The L-P and P-L titration assays devised in this and the previous section provide information about the onset and energies of specific membrane-peptide interactions in a simple manner, which to our knowledge makes this method unique among those employed in studies of membrane pore formation (8).

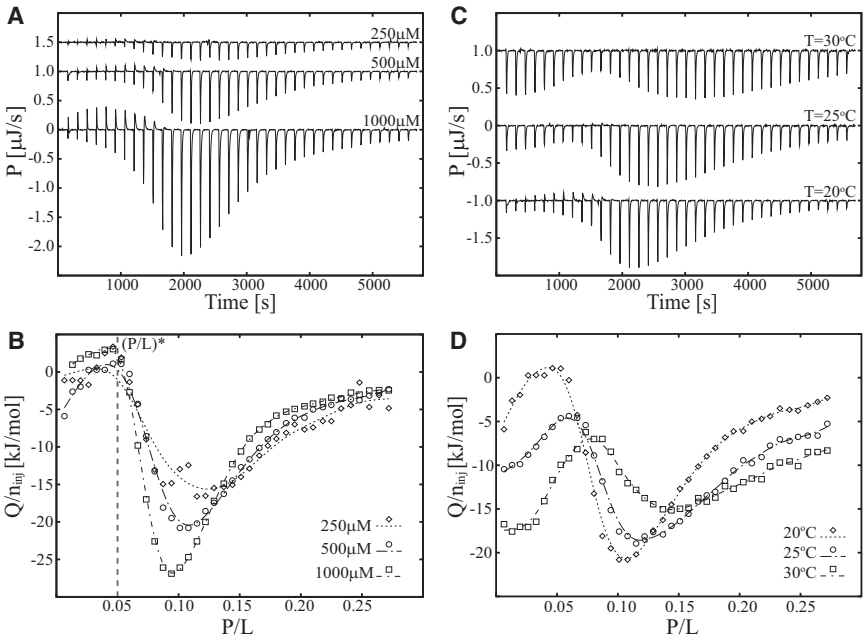

FIGURE 4 ITC heat traces of MPX injected into POPC/POPG (3:1) LUVs at three temperatures and three peptide and lipid concentrations. (*A* and *B*) Calorimetric heat traces (*A*) and normalized heat of injection (*B*) for 250 μM MPX injected into 190 μM LUVs, 500 μM MPX injected into 380 μM LUVs, and 1000 μM MPX injected into 760 μM LUVs at 20°C (38 × 1 μL MPX injections into 204 μL LUVs). (*C* and *D*) Calorimetric heat traces (*C*) and integrated heat of injection (*D*) for 500 μM MPX injected into 380 μM LUVs at 20°C, 25°C, and 30°C (38 × 1 μL MPX injections into 204 μL LUVs). The pore-formation onset, $(P/L)^*$, is indicated by a vertical dashed line in *B*. The integrated heat of injection (Q) has been normalized with respect to the moles of injected peptide (n_{inj}). Lines in *B* and *D* serve to guide the eye.

Thermodynamic profiling of MPX by ITC and cryo-TEM imaging

To this point, the occurrence of pores formed by MPX peptide interacting with POPC/POPG (3:1) lipid membranes has been argued by the signature of a reversible process in the ITC heat trace of the P-L titrations. This argument was substantiated by DLS and SLS measurements that showed that liposomes were still the dominant structure in the studied concentration of MPX, which indicates that membrane solubilization/micellation was not the dominant process investigated. So far, this argumentation applies to the ITC studies conducted at the lipid concentrations $C_{lip} \leq 0.75$ mM. To substantiate our general hypothesis of pore formation, cryo-TEM was employed to map out the membrane morphology at different P/L ratios, which showed special features in the ITC calorimetric heat trace. To obtain the best statistical evaluation of a sample's morphology using cryo-TEM imaging, high lipid concentrations are an advantage. Thus, P-L titrations were conducted by injecting 10 mM MPX into 7.5 mM LUVs at 25°C. For the range $P/L \in [0{:}0.15]$, the 7.5 mM LUV titration profile (Fig. 5 *B*) is similar to the profiles presented in Fig. 4, but beyond the ratio $P/L = 0.15$, the profiles deviate. This difference is observed directly in Fig. 5 *B*, where the 0.75 mM LUV titration shows a smooth progression in heat toward a steady base level of −5 kJ/mol and the 7.5 mM LUV titration shows an increase in heat toward a base level of −17 kJ/mol, with a distinct signature at $P/L = 0.24$. The behavior of the system thus changes in the range $P/L \in [0.15{:}0.30]$ as the lipid concentration is raised from 0.75 mM to 7.5 mM, and this crossover is illustrated by the vertical dashed line in Fig. 5 *B* at $P/L = 0.15$. The lipid-concentration-dependent crossover at $P/L = 15$ is defined as the point where the 0.75 mM and 7.5 mM titrations start to deviate. Cryo-TEM images were recorded at P/L ratios of 0, 0.025, 0.06, 0.12, 0.24, and 0.60 (marked by the letters A–G, respectively, in Fig. 5 *B*). The membrane morphology was inspected in 10–20 images for each P/L ratio and representative images of the sample are shown in Fig. 6.

At P/L ratios 0 and 0.025, peptide partitioning occurs, and 100 to 150 nm LUVs are found (by cryo-TEM) to be the main morphology (Fig. 6, *A* and *B*), as anticipated by the ITC trace in Fig. 5. In this range, the liposomes mainly appear spherical or prolate in shape, with high contrast at the edge allowing for easy detection of the bilayer thickness. At P/L ratios 0.06 and 0.12, 100 to 150 nm LUVs are again observed (by cryo-TEM) as the dominating morphology (and no micelles are observed, in agreement with the DLS and SLS results), but a roughening of the membrane is observed (Fig. 6, *C* and *D*) compared to the smooth membranes shown in Fig. 6, *A* and *B* (examples are presented in higher magnification in Fig. 6, *H* and *I*). This contrast modulation of the liposome edge can be explained

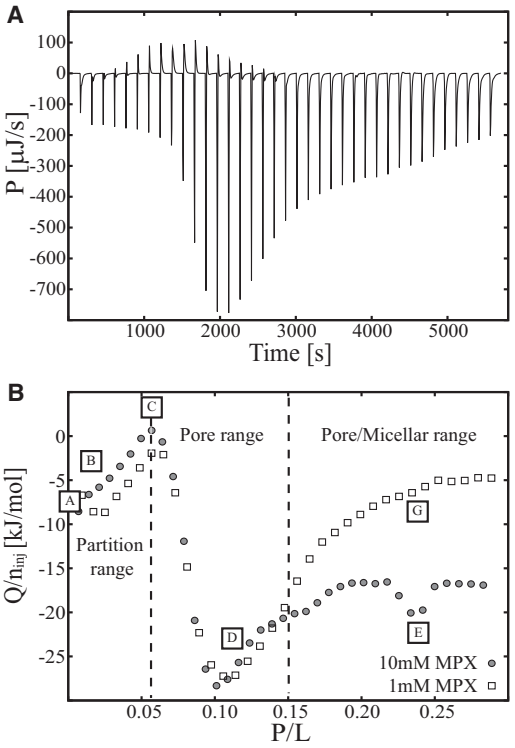

FIGURE 5 ITC heat trace of MPX interacting with POPC/POPG (3:1) LUVs conducted at 25°C. (*A*) Calorimetric heat trace of 10 mM MPX peptide solution injected into 7.5 mM LUVs (38 × 1 μL MPX injections into 204 μL LUVs). (*B*) Heat (Q) normalized with respect to the moles of injected peptide (n_{inj}) for 1 mM and 10 mM MPX titrated into 0.75 mM and 7.5 mM LUVs, respectively. In *B*, the heat trace has been divided into three sections: a partition range, a pore range, and a pore/micellar range. Letter labels *A*–*G* correspond to certain peptide/lipid ratios (P/L) that were analyzed by cryo-TEM.

by the presence of aqueous holes in the membrane (peptide pores), which are clearly visible in the magnification shown in Fig. 6 *H*. Beside the rough edge of the liposome, the membrane region inside the dark rim shows a fenestration, which can be attributed to the presence of low-contrast aqueous holes in the bilayer. Similar findings have been reported for the interaction of magainin with DMPC/DMPG (3:1) lipid membranes (20). The contrast modulation of the membrane is more pronounced for the 0.12 than for the 0.06 P/L ratio due to a higher density of pores in the membrane. The increased pore density at P/L = 0.12 compared to P/L = 0.06 moreover induces a change in the LUV shape, which is evident by the largely nonspherical LUVs shown in Fig. 6 *D*.

Increasing the peptide/lipid ratio further ($P/L > 0.1$) leads to a decrease in the calorimetric heat trace, as observed earlier (Fig. 4), but in the 7.5 mM P-L ITC experiment (Fig. 5), a second signature appears at $P/L = 0.24$, which coincides with the formation of wormlike micelles (Fig. 6 *E*). At higher P/L ratios, the wormlike micelle structure is disrupted, and only globular micelles persist (Fig. 6 *F*). A cryo-TEM study of the composition $P/L = 0.24$ at

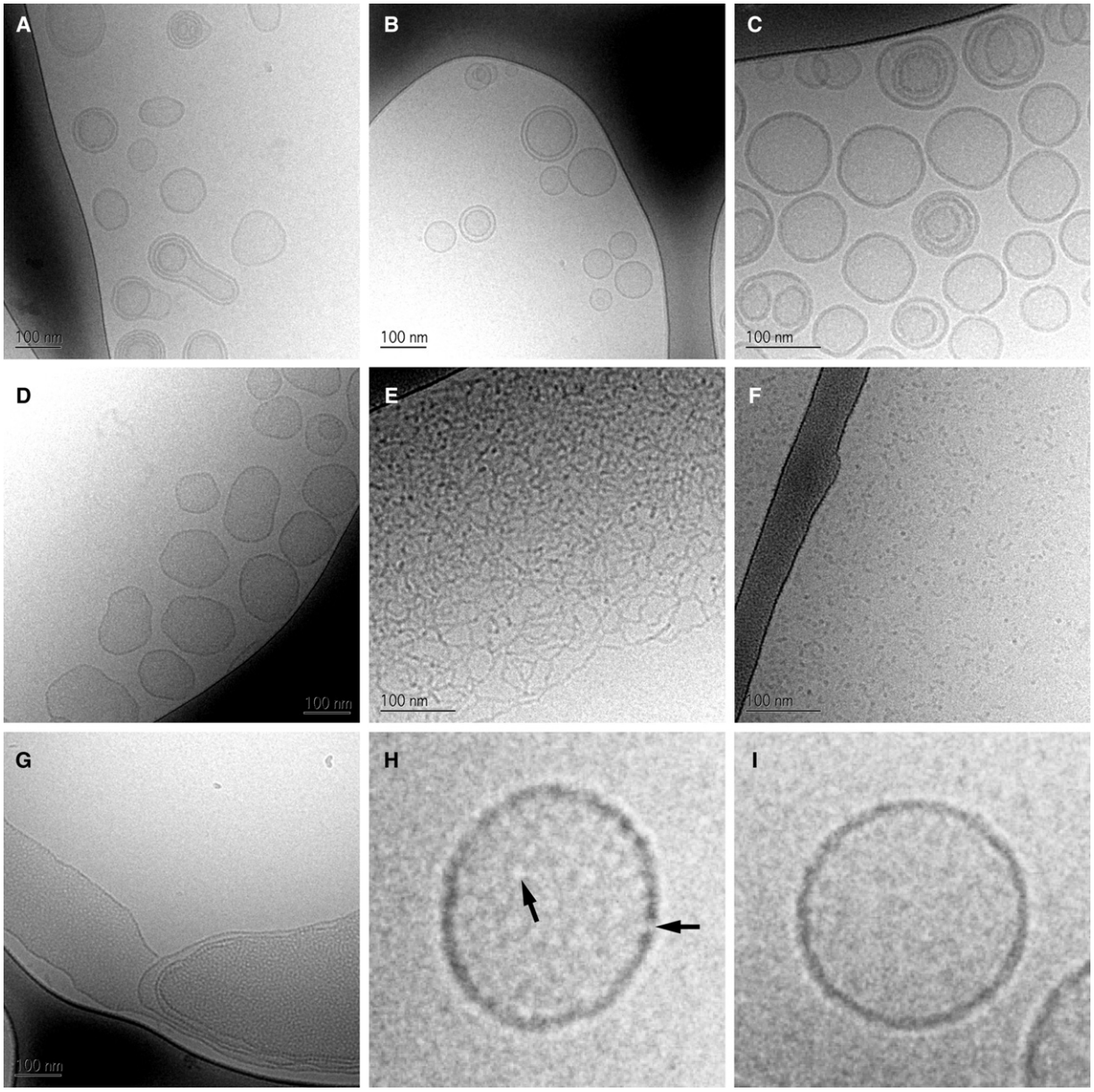

FIGURE 6 Cryo-TEM images of MPX peptide and POPC/POPG (3:1) lipid aggregates vitrified at 25°C. (*A* and *B*) Uni- and multilamellar liposomes with an average size of ~100 nm are shown at $P/L = 0$, $C_{lip} = 7.5$ mM (*A*) and $P/L = 0.025$, $C_{lip} = 7.5$ mM (*B*). (*C* and *D*) The presence of membrane pores is observed at $P/L = 0.06$, $C_{lip} = 7.5$ mM (*C*) and $P/L = 0.12$, $C_{lip} = 7.5$ mM (*D*), where fenestration of the liposome membrane and patterning of the liposome interior can be seen. (*E* and *F*) At higher peptide/lipid ratios, the peptide-lipid aggregates change morphology from lamellar to networks of wormlike micelles (*E*) ($P/L = 0.24$, $C_{lip} = 7.5$ mM) or globular micelles (*F*) ($P/L = 0.60$, $C_{lip} = 7.5$ mM). (*G*) A fenestrated multilamellar membrane system can be seen at $P/L = 0.24$, $C_{lip} = 0.75$ mM. (*H* and *I*) Magnifications of the vesicles imaged in *D* and *A*, respectively. Arrows in *H* point to positions on the membrane with diminished contrast, attributed to aqueous pores spanning the membrane.

$C_{lip} = 0.75$ mM showed the existence of liposomes and larger membrane structures with closely packed pores (Fig. 6 *G*). No wormlike or globular micelles were observed at this lipid concentration contrary to the cryo-TEM studies conducted for the 7.5 mM lipid concentration samples. Together, these results point to the conclusion that, for the range $P/L \in [0.15{:}0.30]$, the system changes behavior from membrane pore formation to membrane micellation as the lipid concentration is increased, and the region is designated as the pore/micelle range in Fig. 5 *B*. As the boundary of the pore/micelle range depends on the lipid concentration, it is more loosely defined than the pore-formation onset at $P/L = 0.05$. Thus, we have found that the ITC heat trace provides a thermodynamic profile of morphological changes in the membrane, thereby providing P/L ratios that are particularly interesting for further study. Observations of globular and wormlike micelles have earlier been reported for lipid/detergent and peptide/lipid systems (12,35). The

observed morphological change from lamellar to micelle structures for increased P/L ratios can be explained either by mechanical instability of the lipid membrane (31) or by geometric packing considerations (12,36).

The contrast modulation observed for the samples shown in Fig. 6, *D*, *E*, and *G*, were further investigated by power-spectra analysis (Fig. 7). Comparison of the power spectra of the membranes (Fig. 6, *D* and *G*) and aqueous background revealed a significant difference for spatial frequencies in the range $S \in [0.005\ \text{Å}^{-1}; 0.015\ \text{Å}^{-1}]$, corresponding to a characteristic lengthscale of 66–200 Å. The power spectrum of the wormlike micelle structure revealed a broader peak in the range $S \in [0.003\ \text{Å}^{-1}; 0.020\ \text{Å}^{-1}]$, which originates from the more disordered packing of this structure. Furthermore, the structure observed for $P/L = 0.12$, $C_{lip} = 7.5$ mM has a characteristic lengthscale similar to that of the structure found for $P/L = 0.24$, $C_{lip} = 0.75$ mM. This finding substantiates the hypothesis that these systems are alike, pointing to the conclusion that the process indeed saturates beyond $P/L = 0.10$ for $C_{lip} = 0.75$ mM, which is also indicated by the declining heat in the ITC trace shown in Fig. 5 *A*. The characteristic lengthscales observed for the MPX system agree with observations by Ludtke and co-workers (20), who reported similar power spectra for DMPC/DMPG liposomes interacting with magainin. In that work, the main peak of the power spectra was attributed to the mean distance between the pores (or holes in the membrane) (20). To address the position of the main peak, cryo-TEM images should be acquired at several P/L ratios within the pore range, leading to defined changes in the main peak in the power spectra. However, such a study lies outside the focus of this work.

CONCLUSION

A model-independent ITC-based methodology for studying membrane pore formation and membrane micellation has been developed and utilized for studying the morphology of POPC/POPG (3:1) LUVs interacting with the antimicrobial peptide MPX. Lipid-into-peptide and peptide-into-lipid titrations were conducted that revealed the occurrence of a reversible process, confirmed by cryo-TEM imaging to be pore formation and further substantiated by DLS/SLS. Pore-formation onset was estimated to $(P/L)^* = 0.05$, and upper and lower limits on the pore-formation enthalpy were determined to be $\Delta H^{up} = -19$ kJ/mol and $\Delta H^{low} = -13$ kJ/mol at $T = 20°C$. The threshold for pore formation given by $(P/L)^*$ was shown to be independent of the lipid concentration but dependent on the temperature. It was found that peptide partitioning was a dominant process for peptide/lipid ratios of $P/L < 0.05$, and peptide pore formation was established to occur in the P/L range $0.05 < P/L < 0.15$. It is interesting that the pore range was succeeded by a micellation range in which both wormlike and globular micelles were observed when $C_{lip} = 7.5$ mM. MPX is thus capable of 1), inserting peripherally into the bilayer; 2), forming pores in the membrane; and 3), inducing membrane collapse into mixed peptide-lipid micelles depending on the P/L ratio and lipid concentration. Furthermore, power-spectra calculations of cryo-TEM images acquired in the pore range $0.05 < P/L < 0.15$ substantiated the occurrence of a characteristic lengthscale, which was attributed to the distance between pores.

The ITC method presented in this work is highly versatile, allowing studies of any peptide and lipid membrane without labeling of the interacting partners. Herein, it has been established how the ITC heat trace can provide structural transition profiles that can be used to identify different processes. Examples are the signature of peptide partitioning, pore formation, and membrane destabilization resulting in the formation of micelles. In general, the technique is a highly valuable tool for pinpointing peptide/lipid ratios (regions of interest) where the system changes behavior, e.g., from peripheral insertion of the peptide to pore formation. These regions of interest can subsequently be investigated/characterized by complementary techniques such as cryo-TEM, NMR, small-angle neutron scattering, small-angle x-ray scattering, or fluorescence assays, thereby elucidating the underlying behavior of the system. An advantage of the ITC approach is that the regions of interest can be accessed for the concentrations and conditions used by the complementary technique. This eliminates problems of

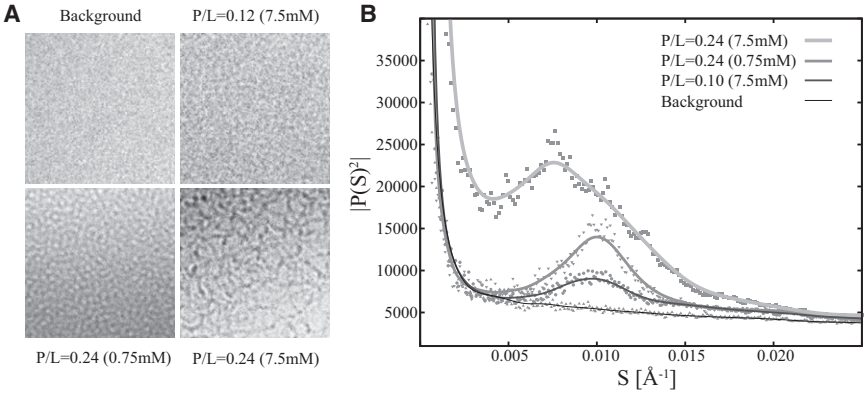

FIGURE 7 (*A*) Cryo-TEM images of the aqueous background, membrane pores, and wormlike micelles. (*B*) Power spectra as a function of the spatial frequency, *S*, of the images in *A*.The spectra for cryo-TEM images acquired at $P/L = 0.12$ at $C_{lip} = 7.5$ mM and $P/L = 0.24$ at $C_{lip} = 0.75$ mM show a distinct peak above the background at $S \in [0.005\ \text{Å}^{-1}; 0.015\ \text{Å}^{-1}]$. This main peak corresponds to a characteristic length of 66–200 Å, which is attributed to the presence of pores in the membrane. The wormlike structure ($P/L = 0.24$ at $C_{lip} = 7.5$ mM) shows a broader peak (*B*), corresponding to a more disordered structure.

relating observations established at different lipid concentrations, which often cause discrepancies due to differences in the fraction of partitioned peptide.

The ITC approach shows great potential to screen antimicrobial peptides for their mode of action toward model lipid membranes. In addition, the approach can also be used to study reconstituted membranes, allowing for a direct investigation of the mode of action of the peptides on cellular lipid membranes.

We thank Lene Hubert and Gunnel Karlsson for valuable technical assistance. Peter Westh and John H. Ipsen are acknowledged for sharing insights on ITC and antimicrobial peptides.

Financial support was kindly provided by the Technical University of Denmark (DTU) and the NanoMorph consortium funded by the Danish Council for Technology and Innovation.

REFERENCES

1. Wieprecht, T., O. Apostolov, …, J. Seelig. 1999. Thermodynamics of the α-helix-coil transition of amphipathic peptides in a membrane environment: implications for the peptide-membrane binding equilibrium. *J. Mol. Biol.* 294:785–794.
2. Klocek, G., T. Schulthess, …, J. Seelig. 2009. Thermodynamics of melittin binding to lipid bilayers. Aggregation and pore formation. *Biochemistry.* 48:2586–2596.
3. Oren, Z., and Y. Shai. 1998. Mode of action of linear amphipathic α-helical antimicrobial peptides. *Biopolymers.* 47:451–463.
4. Wieprecht, T., M. Beyermann, and J. Seelig. 1999. Binding of antibacterial magainin peptides to electrically neutral membranes: thermodynamics and structure. *Biochemistry.* 38:10377–10387.
5. Matsuzaki, K., K. Sugishita, …, K. Miyajima. 1995. Molecular basis for membrane selectivity of an antimicrobial peptide, magainin 2. *Biochemistry.* 34:3423–3429.
6. Chen, F. Y., M. T. Lee, and H. W. Huang. 2003. Evidence for membrane thinning effect as the mechanism for peptide-induced pore formation. *Biophys. J.* 84:3751–3758.
7. Lee, M. T., W. C. Hung, …, H. W. Huang. 2008. Mechanism and kinetics of pore formation in membranes by water-soluble amphipathic peptides. *Proc. Natl. Acad. Sci. USA.* 105:5087–5092.
8. Wenk, M. R., and J. Seelig. 1998. Magainin 2 amide interaction with lipid membranes: calorimetric detection of peptide binding and pore formation. *Biochemistry.* 37:3909–3916.
9. Ladokhin, A. S., and S. H. White. 2001. 'Detergent-like' permeabilization of anionic lipid vesicles by melittin. *Biochim. Biophys. Acta.* 1514:253–260.
10. Ladokhin, A. S., M. E. Selsted, and S. H. White. 1997. Sizing membrane pores in lipid vesicles by leakage of co-encapsulated markers: pore formation by melittin. *Biophys. J.* 72:1762–1766.
11. Yang, L., T. A. Harroun, …, H. W. Huang. 2001. Barrel-stave model or toroidal model? A case study on melittin pores. *Biophys. J.* 81: 1475–1485.
12. Shimada, T., S. Lee, …, M. Tirrell. 2009. Wormlike micelle formation in peptide-lipid conjugates driven by secondary structure transformation of the headgroups. *J. Phys. Chem. B.* 113:13711–13714.
13. Huang, H. W. 2006. Molecular mechanism of antimicrobial peptides: the origin of cooperativity. *Biochim. Biophys. Acta.* 1758:1292–1302.
14. Shai, Y. 1999. Mechanism of the binding, insertion and destabilization of phospholipid bilayer membranes by α-helical antimicrobial and cell non-selective membrane-lytic peptides. *Biochim. Biophys. Acta.* 1462:55–70.
15. Terrone, D., S. L. W. Sang, …, J. R. Silvius. 2003. Penetratin and related cell-penetrating cationic peptides can translocate across lipid bilayers in the presence of a transbilayer potential. *Biochemistry.* 42:13787–13799.
16. Binder, H., and G. Lindblom. 2003. Charge-dependent translocation of the Trojan peptide penetratin across lipid membranes. *Biophys. J.* 85:982–995.
17. Epand, R. F., L. Maloy, …, R. M. Epand. 2010. Amphipathic helical cationic antimicrobial peptides promote rapid formation of crystalline states in the presence of phosphatidylglycerol: lipid clustering in anionic membranes. *Biophys. J.* 98:2564–2573.
18. Epand, R. F., W. L. Maloy, …, R. M. Epand. 2010. Probing the "charge cluster mechanism" in amphipathic helical cationic antimicrobial peptides. *Biochemistry.* 49:4076–4084.
19. Arbuzova, A., and G. Schwarz. 1999. Pore-forming action of mastoparan peptides on liposomes: a quantitative analysis. *Biochim. Biophys. Acta.* 1420:139–152.
20. Han, M. Y., Y. Mei, …, S. J. Ludtke. 2009. Characterization of antibiotic peptide pores using cryo-EM and comparison to neutron scattering. *Biophys. J.* 97:164–172.
21. Ludtke, S. J., K. He, …, H. W. Huang. 1996. Membrane pores induced by magainin. *Biochemistry.* 35:13723–13728.
22. He, K., S. J. Ludtke, …, H. W. Huang. 1996. Mechanism of alamethicin insertion into lipid bilayers. *Biophys. J.* 71:2669–2679.
23. Huang, H. W., F. Y. Chen, and M. T. Lee. 2004. Molecular mechanism of peptide-induced pores in membranes. *Phys. Rev. Lett.* 92:198304.
24. Lee, M. T., W. C. Hung, …, H. W. Huang. 2005. Many-body effect of antimicrobial peptides: on the correlation between lipid's spontaneous curvature and pore formation. *Biophys. J.* 89:4006–4016.
25. Wimley, W. C., M. E. Selsted, and S. H. White. 1994. Interactions between human defensins and lipid bilayers: evidence for formation of multimeric pores. *Protein Sci.* 3:1362–1373.
26. Heerklotz, H., G. Lantzsch, …, A. Blume. 1996. Thermodynamic characterization of dilute aqueous lipid/detergent mixtures of POPC and $C_{12}EO_8$ by means of isothermal titration calorimetry. *J. Phys. Chem.* 100:6764–6774.
27. Hirai, Y., M. Kuwada, …, T. Nakajima. 1979. A new mast cell degranulating peptide homologous to mastoparan in the venom of Japanese hornet (*Vespa xanthoptera*). *Chem. Pharm. Bull. (Tokyo).* 27:1945–1946.
28. Etzerodt, T., J. R. Henriksen, …, T. L. Andresen. 2011. Selective acylation enhances membrane charge sensitivity of the antimicrobial peptide mastoparan-x. *Biophys. J.* 100:399–409.
29. Schwarz, G., and R. Reiter. 2001. Negative cooperativity and aggregation in biphasic binding of mastoparan X peptide to membranes with acidic lipids. *Biophys. Chem.* 90:269–277.
30. Pace, C. N., F. Vajdos, …, T. Gray. 1995. How to measure and predict the molar absorption coefficient of a protein. *Protein Sci.* 4:2411–2423.
31. Henriksen, J. R., T. L. Andresen, …, J. H. Ipsen. 2010. Understanding detergent effects on lipid membranes: a model study of lysolipids. *Biophys. J.* 98:2199–2205.
32. Almgren, M., K. Edwards, and G. Karlsson. 2000. Cryo transmission electron microscopy of liposomes and related structures. *Colloids Surf. A Physicochem. Eng.* 174:3–21.
33. Press, W. H., S. A. Teukolsky, …, B. P. Flannery. 2002. Numerical Recipes in C++: The Art of Scientific Computing, 2nd ed. Cambridge University Press, Cambridge, United Kingdom.
34. Heerklotz, H. H., H. Binder, and H. Schmiedel. 1998. Excess enthalpies of mixing in phospholipid-additive membranes. *J. Phys. Chem. B.* 102: 5363–5368.
35. Edwards, K., J. Gustafsson, …, G. Karlsson. 1993. Solubilization of lecithin vesicles by a cationic surfactant: intermediate structures in the vesicle micelle transition observed by cryo-transmission electron microscopy. *J. Colloid Interface Sci.* 161:299–309.
36. Fattal, D. R., D. Andelman, and A. Benshaul. 1995. The vesicle micelle transition in mixed lipid surfactant systems: a molecular model. *Langmuir.* 11:1154–1161.